Design Exploration and Optimization of a Multi-Corner Crash Box under Axial Loading via Gaussian Process Regression

JUSUF, Annisa, JARWADI, Maulana Hayu, HASTUNGKOROJATI, Dhimaz Galang, GUNAWAN, Leonardo, AKBAR, Mahesa, ZAKARIA, Kemas, IZZATURRAHMAN, Muhammad Faiz and PALAR, Pramudita Satria

International Journal of Technology 15(6) 1749-1770 (2024)
Received September 2024/ Revised September 2024 / Accepted October 2024

International Journal of Technology

http://ijtech.eng.ui.ac.id

Design Exploration and Optimization of a Multi-Corner Crash Box under Axial Loading via Gaussian Process Regression

Annisa Jusuf[1*], Maulana Hayu Jarwadi[2], Dhimaz Galang Hastungkorojati[2], Leonardo Gunawan[3], Mahesa Akbar[4], Kemas Zakaria[2], Muhammad Faiz Izzaturrahman[2], Pramudita Satria Palar[5]

[1]*Mechanics of Solids and Lightweight Structures Research Group, Faculty of Mechanical and Aerospace Engineering, Institut Teknologi Bandung, Bandung 40132, Indonesia*
[2]*Master Program of Aerospace Engineering, Institut Teknologi Bandung, Bandung 40132, Indonesia*
[3]*Dynamics and Control Research Group, Faculty of Mechanical and Aerospace Engineering, Institut Teknologi Bandung, Bandung 40132, Indonesia*
[4]*College of Business, Technology, and Engineering, Sheffield Hallam University, Sheffield S1 1WB, United Kingdom*
[5]*Fluid Dynamics and Propulsion Research Group, Faculty of Mechanical and Aerospace Engineering, Institut Teknologi Bandung, Bandung 40132, Indonesia*

Abstract. Crash box is the most commonly used energy-absorbing systems for increasing transportation safety. Based on this system, design optimization of crash box is important to meeting safety standards with high performance. Therefore, this study aimed to propose a crucial crash box design featuring a 20-corner structure. This new design was expected to increase the number of folds and reduce the size upon impact, which can further elevate specific energy absorption (SEA). In addition, the study implemented a Gaussian Process Regression (GPR) surrogate model for the first time to optimize the multi-corner crash box design. This method reduced the computational cost of the design optimization process while effectively handling complex configurations. The optimization also focused on dimensional parameters such as thickness and perimeter. An explicit nonlinear finite element method was used for axial loading analysis to assess the crash impact performance. The computational results showed good agreement with experimental data where the performance of the 20-corner structure design was compared with other shapes including square, circular, and 12-corner designs. The results showed that the 20-corner structure design provided the most optimum SEA and Crushing Force Efficiency (CFE). Furthermore, the optimized 20-corner design via GPR-model led to a further performance increment with an increase of 8-9% higher SEA and CFE. The following main conclusions can be drawn (i) the cross-sectional geometry significantly influenced crashworthiness performance with the MC20 configuration achieving the best $\boldsymbol{P_m}$, *CFE*, and *SEA* values compared to other configurations. Therefore, the study concluded that the MC20 configuration was the most efficient among the other configurations; (ii) GPR proved advantageous in the optimization process, offering flexibility for complex nonlinear functions, reducing computational costs, and providing error predictions to further refine the optimization model; and (iii) optimization of the MC20 configuration using the GPR surrogate model focused on a single objective which was to maximizing $\boldsymbol{P_m}$.

*Corresponding author's email: annisa.jusuf@itb.ac.id, Tel.: +62222504243
doi: 10.14716/ijtech.v15i6.7278

Keywords: Crashworthiness; Crash box; Design optimization; Gaussian process regression; Multi corner

1. Introduction

Crashworthiness is a critical criterion that should be considered in designing a vehicle (Skhvediani *et al.*, 2023), as it requires vehicle structures to absorb kinetic energy and minimize passengers' injury during an impact collision. Crash box plays a central role in crashworthiness and is positioned between the bumper and side rails in land vehicles. The shape, configuration, and size of a crash box are key determinants of the performance. Basic shapes such as rectangular and circular designs have been extensively used while studies on more complex shapes including multi-corner designs have significantly increased over the last two decades to further enhance crashworthiness. This study introduces a crucial multi-corner crash box design aimed at improving energy absorption and crushing force capabilities. An advanced optimization technique is also applied to streamline the design process and enhance crash box performance.

Crash box is often designed as thin-walled columns due to the high energy absorption, ease of manufacturing, and lightweight structure (Olabi, Morish, hashmi, 2007). The crashworthiness of thin-walled columns depends on factors such as material properties, cross-section shape, configuration, wall thickness, and cross-section perimeter (Wu *et al.*, 2017). Among vehicle collisions, frontal impacts typically cause the most severe injuries and fatalities (Bastien, 2014), which has spurred examination into innovative cross-section designs for crash boxes, as evidenced by numerous studies over recent decades (Christensen, 2022).

Several previous crashworthiness studies focus on metal columns such as steel (Xu *et al.*, 2014; Abedrabbo *et al.*, 2009) and aluminum (Shahi and Marzbanrad, 2012; Galib and Limam, 2004). Recently, studies have expanded to explore columns made from alternative materials, such as composites (Mamalis *et al.*, 2004; Hull, 1991) and hybrid (Wang *et al.*, 2020; Reuter and Tröster, 2017). However, cross-sectional shape and configuration remain important in influencing crashworthiness. Various cross-section shapes have been examined, including square (Lu *et al.*, 2017; Zhang *et al.*, 2014), hexagonal (Alkbir *et al.*, 2014; Hou *et al.*, 2007), octagonal (Liu and Day, 2007), circular (Kumar and Maneiah, 2019; Liu, Huang, and Qin, 2017; Abramowicz and Jones, 1986), top-hat (Dimas *et al.*, 2014; Tarigopula *et al.*, 2006; Schneider and Jones, 2003; White and Jones, 1999), and double-hat shapes (White and Jones, 1999). In addition to these standard cross-sections, unique column shapes such as multi-cell (Lu, Deng, and Liu, 2023; Nagarjun *et al.*, 2020; Zhang *et al.*, 2019; Kumar *et al.*, 2019; Jusuf *et al.*, 2011; Yamashita, Gotoh, Sawairi, 2003; Abramowicz and Wierzbicki, 1989), multi-corner or polygonal (Zhang and Huh, 2010; Zhang and Zhang, 2012; Godat, Legeron, and Bazonga, 2012; Tang, Liu, and Zang, 2012; Liu, *et al.*, 2015; Abbasi *et al.*, 2015; Reddy, Abbasi, and Fard, 2015), and origami-inspired designs (Yuan *et al.*, 2019; Zhou, Zhou, and Wang, 2017) have been developed.

Studies show that increasing the column's thickness can improve the crash box's energy absorption capacity (Qi, Yang, Dong, 2012; Liu, 2008). Alternatively, energy absorption can also be improved through multi-corner column designs, as several studies have shown (Liu *et al.*, 2015; Abbasi *et al.*, 2015; Reddy, Abbasi, and Fard, 2015; Zhang and Zhang, 2012; Godat, Legeron, and Bazonga, 2012; Tang, Liu, and Zang, 2012; Zhang and Huh, 2010). Crashworthiness analysis has been conducted on multi-corner cross-sections, such as rectangular, hexagonal, octagonal, and 12-edge profiles (Abbasi *et al.*, 2015) (Reddy, Abbasi, and Fard, 2015). Results show that columns with a 12-edge profile have higher *SEA* and *CFE* than others, suggesting that increasing the number of corners improves energy

absorption efficiency. Recently, (Zhang *et al.*, 2022) conducted a numerical analysis of energy absorption in 12-corner columns with variable thicknesses and estimated mean crushing force using a theoretical approach derived from plastic deformation theory for thin-walled columns. Results suggest that plastic collapse models for prismatic columns can be applied to multi-corner designs.

Over the last decade, optimization techniques, such as genetic algorithms and artificial neural networks, have become effective tools for enhancing crash box performance. Insights from these optimization studies are crucial for understanding crashworthiness and guiding future design improvements. Various authors have conducted crash box optimizations (Borse, Gulakala, and Stuoffel, 2024; Djamaluddin, 2024; Jongpradist, *et al.*, 2024; Bhutda, Sonje, and Goel, 2023; Wang, *et al.*, 2022; Ciampaglia, *et al.*, 2021; Wang, *et al.*, 2020; Chen, *et al.*, 2019; Pirmohammad and Esmaeili-Marzdashti, 2019; Fang, *et al.*, 2017).

Wu *et al.* (2017) introduced a discrete optimization algorithm using orthogonal arrays to optimize Specific Energy Absorption (*SEA*) in Fourier-section tubes. Chen *et al.* (2019) used multi-objective optimization with surrogate models to identify the optimal design for hybrid multi-cell columns, combining circular and square sections in various configurations. Fang *et al.* (2017) reviewed essential studies and recent developments in structural crashworthiness and energy absorption optimization. Additionally, Pirmohammad and Esmaeili-Marzdashti (2019) optimized hole shapes and sizes in square and octagon thin-walled structures using genetic algorithms (NSGA-II) and artificial neural networks to achieve optimal configurations.

Wang *et al.* (2020) introduced a bionic multi-corner crash box inspired by the structure of the cactus. This multi-objective optimization design is developed using the response surface model (RSM) and Latin hypercube design. Wang *et al.* (2020) showed that the bionic crash box reduced the vehicle damage, increases energy absorption, and creates a stable folding deformation. Wang *et al.* (2022) explored a new hexahedral pyramid crash box, using the RSM and a multi-objective evolutionary algorithm with a detection and escape strategy (MOEA/D-DAE) to improve crash box performance. Results demonstrated that the hexahedral pyramid crash box has superior energy absorption compared to hollow, hexagonal honeycomb, and re-entrant crash boxes. Moreover, the optimized hexahedral pyramid design offers enhanced energy absorption and more stable folding deformation. Recent studies have also examined optimization approaches for advanced designs with complex configurations and innovative materials, such as origami-shaped crash boxes (Ciampaglia *et al.*, 2021), foam-filled designs (Djamaluddin, 2024) and boxes made from functionally graded materials (Jongpradist *et al.*, 2024).

Beyond traditional methods, machine learning has evolved as a valuable approach in design optimization. Gaussian Process Regression (GPR), also known as Kriging surrogate modeling, has gained popularity in engineering for its ability to reduce computational costs while delivering accurate solutions in less time (Palar and Shimoyama, 2019). This model can not only predict outcomes but also provide error estimates, improving Bayesian optimization and further supplying supplementary information in a relatively straightforward manner. GPR's flexibility makes the model ideal for capturing complex, nonlinear responses (Palar, Zuhal, and Shimoyama, 2020).

Previous study outlines the importance of geometric and dimensional factors in enhancing energy absorption for crashworthiness, material deformation, and failure characteristics. Therefore, exploring and optimizing crash boxes with varied cross-sections and dimensions is necessary to understand how these factors impact overall performance. Despite the potential of multi-corner crash boxes, a comprehensive comparison across

different cross-sectional shapes remains unexplored. Studies show that increasing the number of corners enhances energy absorption and *SEA*. Multi-corner crash boxes have been implemented in practical applications, as seen in designs by Ford (Cheng, 2011) and Sumitomo (Nakazawa *et al.*, 2005). This study proposes a new 20-corner multi-corner design, previously unexplored, with shape optimization.

The proposed design features recessed sections on all four sides to increase the number of folds and reduce their size upon impact, enhancing *SEA* values. For future applications, crash boxes could be produced using 3D printing to incorporate complex geometries such as auxetic and lattice structures (Kholil *et al.*, 2023; Hou *et al.*, 2023; Seek *et al.*, 2022).

Basic shapes such as square and circular, are commonly used in crash boxes for ease of manufacture. In this study, a 20-corner design derived from a square cross-section is proposed to maintain manufacturing simplicity. Additionally, other multi-corner shapes, such as a 12-corner H-like and a 12-corner plus sign-like design, are evaluated for comparison. Parametric studies are conducted on shape dimensions, including perimeter and thickness. The crashworthiness parameters—mean crushing force (P_m), *SEA*, and Crushing Force Efficiency (*CFE*)—are analyzed using finite element methods.

The GPR model based on Rasmussen (2003) is implemented to conduct optimization on the design of the 20-corner shape. A fine-tuning of the most efficient cross-section in terms of crashworthiness performance is performed using a Bayesian optimization procedure based on Jones's research (Jones, Schonlau, and Welch, 1998). The GPR-based optimization is particularly effective in approximating nonlinear responses, which are characteristic of the challenges addressed in this study. Additionally, GPR provides point-wise predictive uncertainty, an essential feature for Bayesian optimization, which is not available in models such as artificial neural networks or polynomial regression. This optimization process aims to deliver a high-performance 20-corner configuration based on P_m, offering greater resistance to vehicle structure during frontal impacts while keeping general dimensions within practical limits.

2. Methods

2.1. Crashworthiness characteristics

This study examined three main crashworthiness parameters, namely (1) Mean Crushing Force (P_m), (2) Specific Energy Absorption (*SEA*), and (3) Crushing Force Efficiency (*CFE*).

2.1.1. Mean Crushing Force

Mean crushing force (P_m) represented the total energy absorption (*EA*) divided by the total crushing length (δ_{max}), as shown in Equation 1.

$$P_m = \frac{1}{\delta_{max}} \int_0^{\delta_{max}} P\delta \, d\delta = \frac{EA}{\delta_{max}} \tag{1}$$

Where P denoted the crushing force and δ represented the crushing length (displacement) along the axial direction of the crash box structure. A higher P_m value showed a greater ability of the structural to absorb energy.

2.1.2. Specific Energy Absorption

SEA which was another critical parameter measured the energy absorption efficiency of the crash box. The *SEA* was defined as the total absorbed crash energy (*EA*) divided by the deformed mass of the structure ($m_{deformed}$), as shown in Equation 2.

$$SEA = \frac{1}{m_{deformed}} \int_0^{\delta_{max}} P\delta \, d\delta = \frac{EA}{m_{deformed}} \quad (2)$$

2.1.3. Crushing Force Efficiency

Crushing force efficiency (*CFE*) was the ratio of the P_m to the maximum crushing force (P_{max}), as shown in Equation 3.

$$CFE = \frac{P_m}{P_{max}} \quad (3)$$

Where P_{max} referred to the maximum force which was kept low to reduce the load transmission from the crash box to the vehicle's main body. A high *CFE* implied that the design absorbed energy effectively by maximizing energy absorption while minimizing peak force. In this study, impact behavior of crash box structures was analyzed for P_m, *CFE*, and *SEA* by varying the cross-sectional shapes, thickness, and perimeter.

2.2. GPR Surrogate Model

A surrogate model captured the relationship between the input and output variables, $f(x)$, through an estimated function $\hat{f}(\boldsymbol{x})$, where $\boldsymbol{x} = \{x_1, x_2, \dots, x_m\}^T$ with m being the design variables. The initial step included preparing the design of experiments $\boldsymbol{X} = \{\boldsymbol{x}^{(1)}, \boldsymbol{x}^{(2)}, \dots, \boldsymbol{x}^{(n)}\}^T$ and the corresponding responses $\boldsymbol{y} = \{y^{(1)}, y^{(2)}, \dots, y^{(n)}\}^T = \{f(\boldsymbol{x}^{(1)}), f(\boldsymbol{x}^{(2)}), \dots, f(\boldsymbol{x}^{(n)})\}^T$ where n was the sample size. GPR assumed that the prediction $\hat{f}(\boldsymbol{x})$ was the mean of realizations of Gaussian processes represented by the following Equation 4.

$$\hat{f}(\boldsymbol{x}) = \mu + Z(\boldsymbol{x}), \quad (4)$$

Where $\mu(\boldsymbol{x})$ represented the mean term and $Z(\boldsymbol{x})$ denoted the stochastic process. GPR assumed correlations between different points defined by the correlation function $k(\boldsymbol{x}^{(i)}, \boldsymbol{x}^{(j)})$, as shown in Equation 5.

$$\mathrm{cor}(y^{(i)}, y^{(j)}) = k(\boldsymbol{x}^{(i)}, \boldsymbol{x}^{(j)}), \quad (5)$$

The implementation in this study used the squared-exponential correlation function as shown in Equation 6.

$$k(\boldsymbol{x}^{(i)}, \boldsymbol{x}^{(j)}; \theta) = \exp(-\frac{(x^{(i)} - x^{(j)})^2}{2\theta^2}, \quad (6)$$

Where θ was the lengthscale of the correlation function. In GPR, a k-dimensional correlation function was constructed as a product of one-dimensional components. Thus, lengthscales required tuning, forming a vector $\boldsymbol{\theta} = \{\theta_1, \theta_2, \dots, \theta_m\}$.

To capture correlations among all samples in the design, the $\boldsymbol{\Psi}$ matrix (of size $n \times n$) was constructed, where each component. The (i, j)-th component of the $\boldsymbol{\Psi}$ matrix equals to $\mathrm{cor}(y^{(i)}, y^{(j)}) = k(\boldsymbol{x}^{(i)}, \boldsymbol{x}^{(j)})$. The stochastic term of GPR, $Z(\boldsymbol{x})$, was formulated as follows

$$Z(\boldsymbol{x}) = \psi(\boldsymbol{x})^T \boldsymbol{\Psi}^{-1}(\boldsymbol{y} - 1\mu). \quad (7)$$

Where ψ represented the $n \times 1$ correlation vector between an arbitrary point $\boldsymbol{x}^*$ with the experimental design $\boldsymbol{X}$, $\psi = \{k(\boldsymbol{x}^*, \boldsymbol{x}^{(1)}), k(\boldsymbol{x}^*, \boldsymbol{x}^{(2)}), \dots, k(\boldsymbol{x}^*, \boldsymbol{x}^{(n)})\}^{\boldsymbol{T}}$. The prediction structure of GPR then reads as

$$\hat{y}(\boldsymbol{x}^*) = \mu + \psi(\boldsymbol{x}^*)^T \boldsymbol{\Psi}^{-1}(\boldsymbol{y} - 1\mu) \quad (8)$$

Beside the prediction, GPR also directly provided the uncertainty estimate, as given by

$$\hat{s}^2(\boldsymbol{x}) = \sigma^2 \left[1 - \psi^T \boldsymbol{\Psi}^{-1} \psi + \frac{(1 - 1^T \boldsymbol{\Psi}^{-1} \psi)}{1^T \boldsymbol{\Psi}^{-1} 1}\right] \tag{9}$$

Where σ^2 denoted the GPR variance. The implementation of GPR considered numerical noise by adding a regression factor λ to the correlation matrix. Therefore, the correlation matrix became $\widetilde{\boldsymbol{\Psi}} = \Psi + \lambda \boldsymbol{I}$, where I represented the identity matrix.

The optimum hyperparameters $\gamma = \{\boldsymbol{\theta}, \sigma^2, \lambda\}$ were aimed by minimizing the negative of ln-likelihood function, as shown in Equation 10.

$$\ln(\mathcal{L}) = -\frac{n}{2}\ln 2\pi - \frac{1}{2}\ln|\boldsymbol{\Psi}| - \frac{1}{2}(\boldsymbol{y} - 1\mu)^T \boldsymbol{\Psi} (\boldsymbol{y} - 1\mu) \tag{10}$$

The GPR mean was estimated by the maximum possible estimation. To accomplish the hyperparameter optimization, this study used the combination of genetic algorithm and hill-climbing to increase the chance of finding the global optimum.

Bayesian optimization enriched the experimental data by evaluating a solution that maximized the acquisition function (Jones, Schonlau, and Welch, 1998). The Bayesian optimization was initiated by seeding the design space with initial samples. The formulation of the expected improvement as the acquisition function, given an established GPR prediction at an arbitrary point $\boldsymbol{x}$ as shown in Equation 11.

$$E[I(\boldsymbol{x})] = \left(y_{min} - \hat{f}(\boldsymbol{x})\right)\left[\frac{1}{2} + \frac{1}{2}\left(\frac{y_{min} - \hat{f}(\boldsymbol{x})}{\hat{s}(\boldsymbol{x})\sqrt{2}}\right)\right] + \hat{s}(\boldsymbol{x})\frac{1}{\sqrt{2\pi}}\exp\left[\frac{-\left(y_{min} - \hat{f}(\boldsymbol{x})\right)^2}{2\hat{s}(\boldsymbol{x})^2}\right] \tag{11}$$

Where y_{min} represented the best solution observed (in the context of minimization).

At every iteration of Bayesian optimization, the sample point with the highest $E[I(\boldsymbol{x})]$ (i.e., $\boldsymbol{x}_{opt}$) was found by a genetic algorithm followed by a local search. The $\boldsymbol{x}_{opt}$ was then evaluated by a computer simulation and added to the experimental design. The process was then repeated until the computational budget was exhausted.

3. Numerical Simulation and Optimization Procedures

3.1. Geometrical Detail

In this study, five cross-section configurations were studied, including basic geometries (square 'SQ' and circular 'CR' crash boxes) and more complex, multi-corner geometries, such as 12-corner structures with H-like shapes ('MC12'), 12-corner structures with a positive sign-like shape ('MC12+'), and 20-corner crash boxes ('MC20'), as shown in Figure 1.

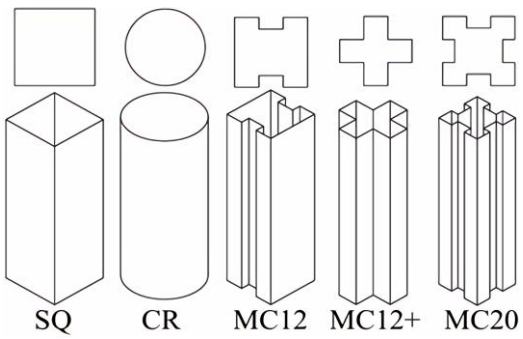

Figure 1 Depictions of various cross-section used in the design exploration phase

The inclusion of basic geometries allowed an observation of the performance gains achieved by the multi-corner designs. Two different square crash boxes were analyzed where the first was labeled as 'SQV' which served to validate the finite element model, and the second called 'SQ' for parametric studies.

Table 1 shows the details of the crash boxes in the study. The first square crash box (SQV) followed experimental studies previously conducted by Jusuf et al. (2011; 2015) and Gunawan (2013). The second square crash box (SQ) was among the five models created with the same mass and length (150 mm), while thickness and perimeter were set as variable design factors. The thickness ranged from 1 to 3 mm, and the perimeter spanned from 120 to 400 mm. The lengths of each side for all cross-sections were adjusted so that the resulting perimeter matched the specified design values.

Table 1 Nomenclature of crash Box

No	Type	Code	Remarks
1	Square	SQV	For Validation
2	Square	SQ	For Parametric Studies
3	Circular	CR	
4	12-corners with H-like shape	MC12	
5	12-corners with + like shape	MC12+	
6	20-corners	MC20	

For fair comparison, side lengths of each cross-section were proportionately adjusted to yield a perimeter equal to the given design values. In MC12, MC12+, and MC20, relationships between side lengths were fixed. For MC12, when the longest side length was defined as $\boldsymbol{a_{mc12}}$, the other sides were set to $\boldsymbol{a_{mc12}/3}$ and $\boldsymbol{a_{mc12}/6}$ (see Figure 2). In MC20, when the longest distance between points on the edge was $\boldsymbol{a_{mc20}}$, the other sides were $\boldsymbol{a_{mc20}/3}$ and $\boldsymbol{a_{mc12}/20}$ (refer to Figure 2).

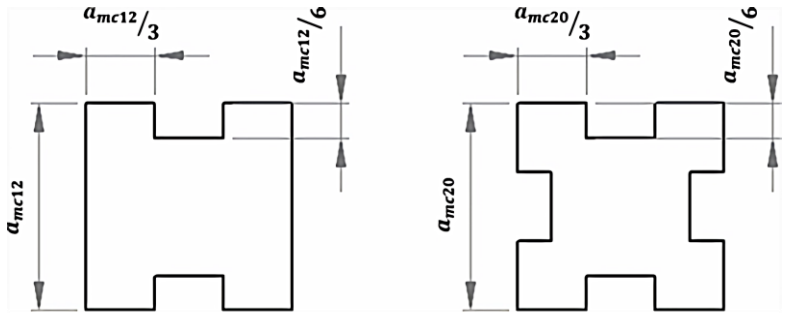

Figure 2 Relationship between side lengths for the MC12 and MC20 crash box used in the design exploration phase

For design exploration, the thickness bounds were set from 1 to 3 mm, and the perimeter bounds from 120 to 400 mm. Thirty-one sampling points were generated using Halton (1964) sampling method. This was joined with an additional four sampling points placed at the corners of the design space.

3.2. Mechanical Properties

The crash box material used was mild steel (St37) with a Young's modulus of 222 GPa, a Poisson's ratio of 0.3, a density of 7.33×10^6 kg/mm^3, a yield strength of 0.29 GPa, and power-law hardening of 0.157. Figure 3 illustrates the true stress-plastic strain curve where the material properties were defined as elastoplastic, accounting for strain rate effects. Due to the material's strain rate sensitivity, Cowper-Symonds parameters D and q were applied, valued at 6844 s^{-1} and 4.12, respectively (Jusuf *et al.*, 2015). Properties for the impactor material included a Poisson ratio of 0.3 and a density of 7.5×10^{-4} kg/mm^3.

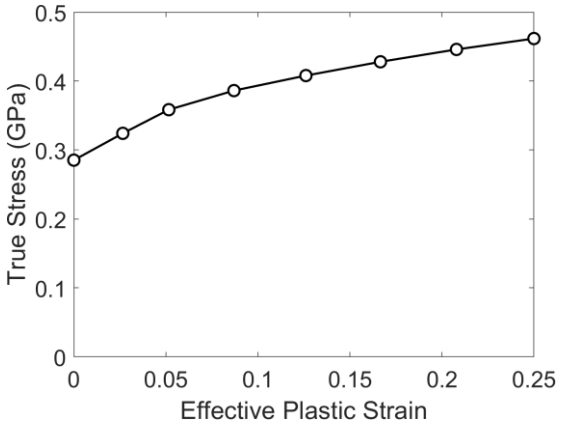

Figure 3 True Stress-Effective Plastic Strain of Mild Steel St37

3.3. Finite Element Modelling and Validation

3.3.1. Finite Element Modelling

The crash box performance analyses were conducted using explicit nonlinear dynamic analysis software. The typical finite element model for crushing analysis of a crash box was depicted in Figure 4. A crash box was modelled as a thin-walled column subjected to the axial impact loading through the impactor. The impactor mass was 30 kg, modelled as a rigid body to avoid energy absorption on the impactor. The impactor could translate freely in the axial direction while constrained in other directions, with a velocity of 10 m/s in the negative y-direction as shown in Figure 4. The lower end of the column was made as a fixed constraint which implied that there was no translation and rotation in any direction, as depicted in Figure 4. The column material was modelled using a piecewise linear plasticity because the column was expected to absorb energy by the plasticity mechanism.

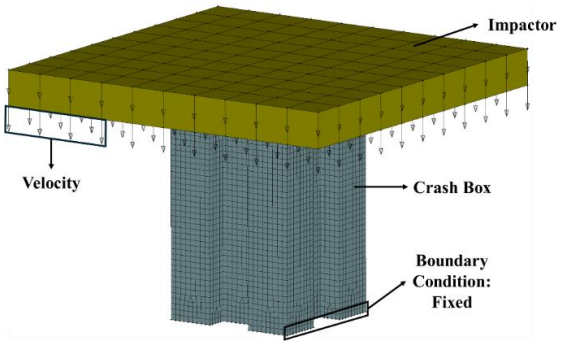

Figure 4 The typical crash box model in the finite element simulation

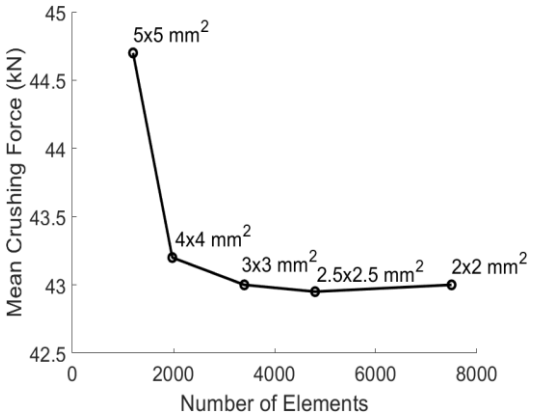

Figure 5 Result of mesh convergence study

The column walls were modelled using quad-node shell elements. To specify the element size, a convergence test was performed by varying the size of the mesh elements in a square column with a perimeter of 200 mm and a thickness of 1 mm. The result showed that the scheme with a single mesh element of 3×3 mm^2 was adequate to ensure reasonable accuracy, as shown in convergence test outcome in Figure 5. Two contact algorithms were used namely 'automatic nodes to surface' and 'automatic single surface.' The 'automatic nodes to surface' defined the contact between the impactor and the crash box. On the other hand, the 'automatic single surface' contact was applied to avoid self-penetration on the column wall during folding creation. The static and dynamic friction coefficients for all contact mechanisms were 0.4 and 0.3 (Zhang *et al.*, 2019) respectively.

3.3.2. Validation

Validation of the finite element model was conducted using the SQV cross-section, as examined by Jusuf *et al.* (2011; 2015) and Gunawan (2013) to ensure accuracy in the modeling approach. Upon successful validation, the model was employed to analyze and optimize the crash box structures for the study. Table 2 and Figure 6 show a comparison of the crashworthiness characteristics of the validated crash box structure.

Table 2 SQV crashworthiness characteristic comparison

	P_{max} (kN)	δ_{max} (mm)	EA (kJ)	P_m (kN)	CFE	SEA (kJ/kg)	Difference (%)	
							EA	P_m
Numerical*	69.5		1.51	14.21	0.20	11.56	0.38	0.39
Experimental**	56.7	106.10	1.57	14.76	0.26	12.05	3.62	3.37
Validation***	69.5		1.51	14.26	0.21	11.62		

*(Jusuf, *et al.*, 2015); **(Gunawan, 2013); ***Present study

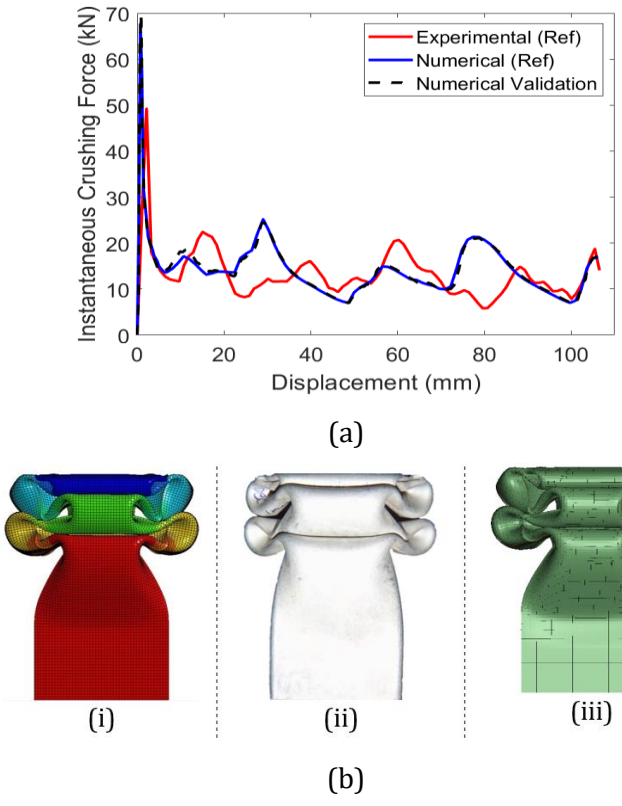

Figure 6 (a) Crushing force response of SQV mild steel square columns, (b) Deformation modes of square columns (i) numerical (Jusuf *et al.*, 2015), (ii) experimental (Gunawan, 2013), (iii) numerical validation

3.4. Design Exploration and Optimization Framework

Before examining the design exploration and optimization results in detail, several preparatory steps were necessary to ensure that the simulated samples could be optimized using the GPR surrogate model. As explained in Section 3.1, there were variations in thickness (Δ) and perimeter (ζ) values across five cross-sectional configurations, which were detailed in Table 1. A finite element crash box simulation was then performed for each variation in thickness and perimeter for all configurations. From this simulation process, an instantaneous force graph was obtained and processed to determine the crash box performance parameters namely P_m, *CFE*, and *SEA*, which could be calculated using the equation in Section 2.1. The influence of perimeter and thickness on the three crashworthiness characteristics was further analyzed based on these results. In particular, the most efficient cross-section in terms of the mentioned metrics was determined from this procedure. Additionally, the trade-off between the three-performance metrics was also made visible with the help of GPR. The instantaneous and mean crushing forces of the solutions of interest were also analyzed to identify important design insights.

After completing the design exploration, Bayesian optimization was applied to identify the most efficient cross-sectional configuration. Using the MC20 configuration results as input, the GPR model was employed to perform the optimization process to determine when further improvements were possible. The Kriging-based optimization algorithm then fine-tuned the crash box geometry by fixing perimeter and thickness values to their optimal levels. This process identified an optimal geometry by refining these geometric details, with the initial perimeter and thickness values of the cross-section having the highest P_m serving as the baseline design. The primary aim was to maximize the crash box's potential in terms of mean crushing force (P_m) P_m. Finally, the optimal P_m value from this optimization was compared with simulation results for the optimal configuration, allowing for an assessment of performance improvement after fine-tuning.

4. Results and analysis

4.1. Design exploration result

The analysis began with design exploration results to evaluate how cross-sectional shapes influenced crash box performance, as outlined in Table 1. The GPR plots for P_m, *CFE*, and *SEA*, illustrated through surface and contour plots in Figures 7, 10, and 11, respectively, show trends between thickness and perimeter values and crashworthiness characteristics for each configuration. These trends were derived using Gaussian regression based on the simulation results of 35 samples, each with consistent variation distributions for different configurations. The contours and color gradients in the GPR plots indicate how crashworthiness metrics varied with changes in perimeter and thickness, providing a clear view of these factors' effects. From the GPR plots, the minimum and maximum values of P_m, *CFE*, and *SEA* for each cross-section were summarized in Table 3.

4.1.1. Comparison based on P_m

Figure 7 showed that the cross-sectional shape significantly affected the structural impact behaviour with each cross-section generating unique P_m values.

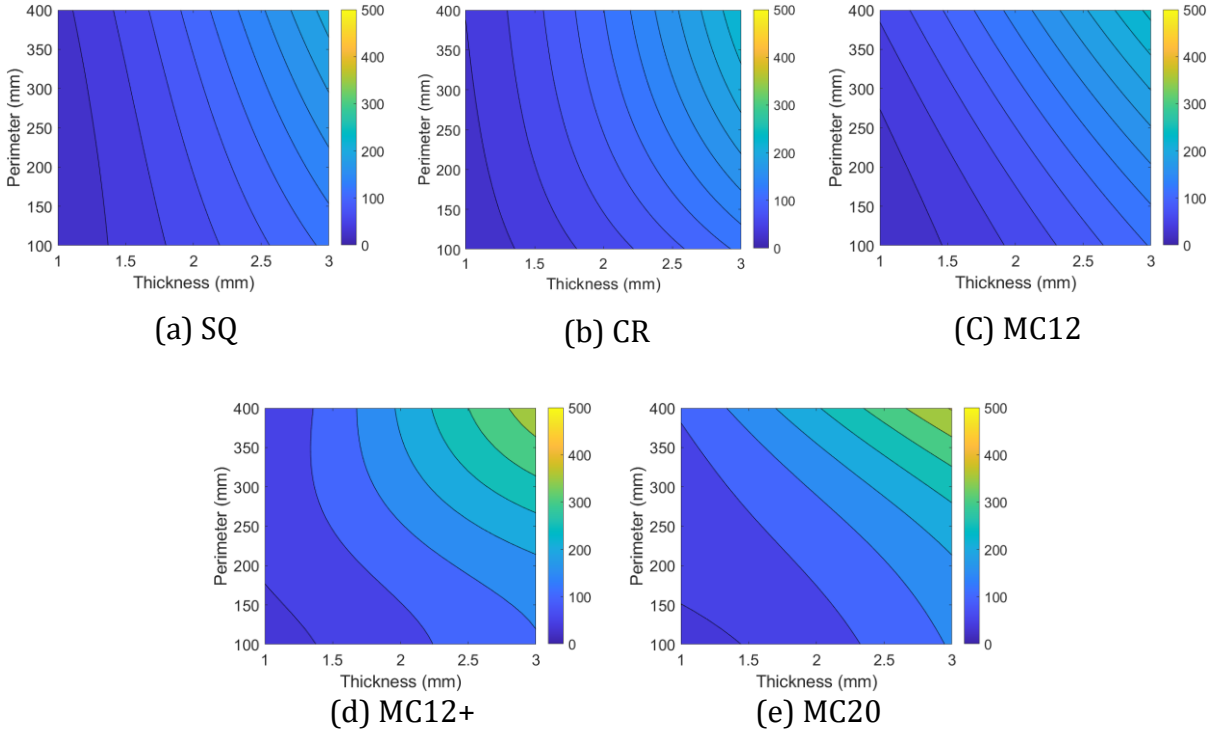

Figure 7 GPR plots for the P_m of the five cross-sectional shapes

The first clear trend observed was that increasing thickness and perimeter generally led to higher mean crushing forces across all cross-section types. The second trend showed that, for all configurations, the optimal P_m value was achieved at Δ = 3 mm and ζ = 400 mm, a pattern consistent across crash box types (as depicted in Figures 7(a) to 7(e)).

Figure 8 presented the instantaneous crushing force versus crushing length and the mean crushing force versus crushing length for all cross-sections with the maximum P_m (ζ = 400 mm, Δ = 3 mm). In Figure 8(a), differences in instantaneous force trends showed variations in each configuration's ability to withstand impact forces, which consequently influenced mean crushing force values displayed in Figure 8(b). Comparing configurations with the same perimeter and thickness, it was evident that certain cross-sectional shapes performed better. At maximum perimeter and thickness, the MC12, MC12+, and MC20 configurations suggested higher mean crushing forces than the SQ and CR shapes, with MC20 achieving the highest P_m and SQ the lowest. This trend further suggested that increasing the number of corners improves performance in terms of mean crushing force.

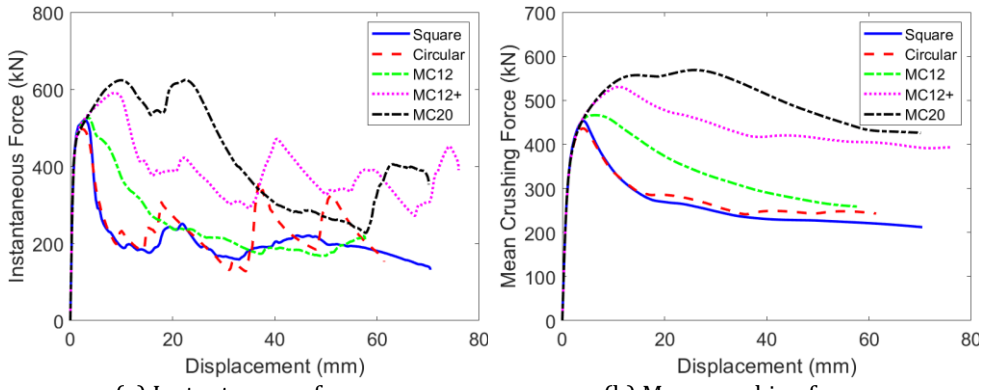

Figure 8 Instantaneous and Mean Crushing Force for the Maximum $\boldsymbol{P_m}$ Configurations ($\boldsymbol{\zeta}$ = 400 mm, Δ = 3 mm)

The mean crushing force was found to be more sensitive to changes in thickness than perimeter. Interestingly, the circular (CR) shape, which theoretically represents a crash box with infinite corners, did not perform as well as the multi-corner shapes in terms of mean crushing force (P_m). Even with the same number of corners, MC12+ outperformed MC12 and further outlined that geometry played a crucial role in performance. Progressive buckling occurred across all shapes during deformation with SQ, CR, and MC12 forming longer wavelength folds. On the other hand, MC12+ and MC20 developed shorter wavelength folds which enabled the elements to absorb more energy. The deformation patterns of each crash box shape revealed significant differences in crashworthiness performance, as shown in Figure 9.

The SQ shape exhibited progressive buckling, while the CR shape displayed smooth, uniform deformation. In contrast, the multi-cell configurations (MC12, MC12+, and MC20) showed complex folding and buckling, enhancing load distribution and energy absorption. These findings suggested that a crash box's performance depends not only on corner count but also on the geometry of the multi-corner section. Specifically, increasing thickness, perimeter, and the number of corners led to shorter fold wavelengths, contributing to a higher P_m and improved energy absorption. Although MC20 achieved the highest P_m value, further optimization is recommended to enhance its design.

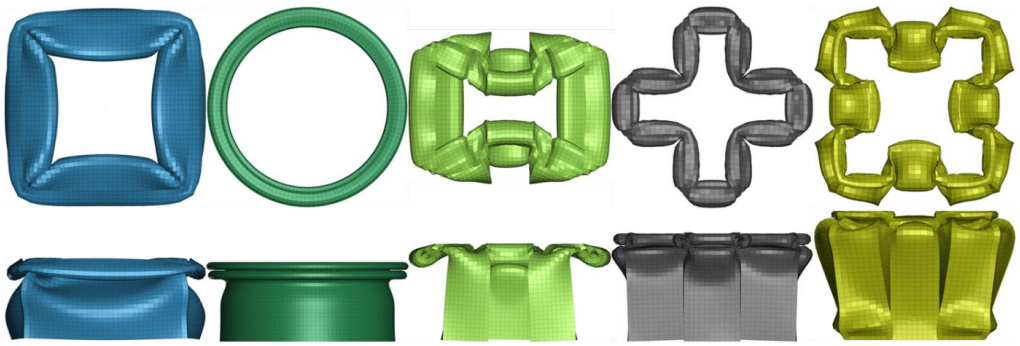

Figure 9 Deformed shapes at maximum $\boldsymbol{P_m}$ ($\boldsymbol{\zeta}$ = 400 mm, Δ = 3 mm)

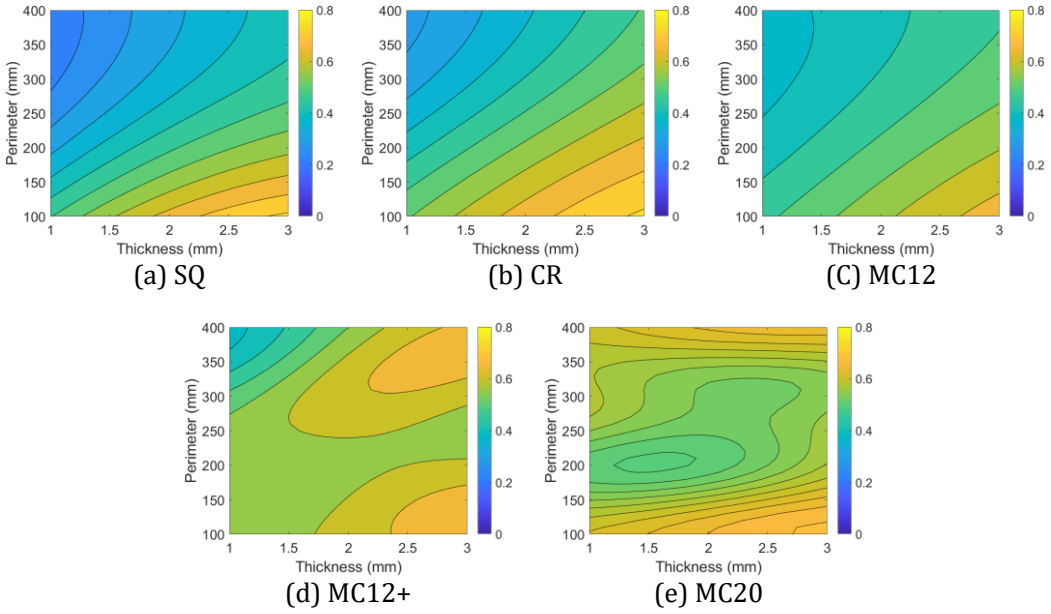

Figure 10 GPR Plots for the ***CFE*** of the five cross-sectional shapes

4.1.2. Comparison based on *CFE*

Figure 10 presented the GPR plots for *CFE* across all crash box configurations, similar to Figure 7, which showed the impact of variations in thickness and perimeter on crashworthiness characteristics. For simple shapes (SQ, CR, MC12), results showed that increasing thickness while reducing perimeter improved *CFE*, as shown in Figures 10(a) through 10(c). Significantly, a trade-off evolved between *CFE* and mean crushing force P_m. This trade-off implied maximizing *CFE* would lead to reduced performance in terms of P_m and P_{max}, (refer to Equation 3).

Although simple shapes such as SQ, CR, and MC12 showed a steady increase in *CFE* with greater thickness and smaller perimeter, the trend was more complex for MC12+ and MC20. This complexity implied that configuring perimeter and thickness for MC12+ and MC20 required caution, as the relationship with *CFE* did not follow a simple trend, especially for MC20. Results also showed that although CR achieved the highest possible *CFE* among the cross-sections, this advantage was minimal compared to the others. Furthermore, Figure 10 suggested a contrasting *CFE* trend for MC12+ and MC20 compared to the simpler shapes. Simple shapes saw increased *CFE* with higher thickness and lower perimeter, while MC12+ and MC20 displayed two local maximum values, nearly equal in peak, as indicated in Figures 10(d) and 10(e). Furthermore, Table 3 showed that MC20's *CFE* slightly outperformed MC12+.

4.1.3. Comparison Based on SEA

As shown in Figure 11, high *SEA* was achieved by reducing perimeter and increasing thickness in simpler shapes (SQ, CR, MC12). This trend mirrored the one for *CFE*, where maximizing thickness and minimizing perimeter led to higher *CFE* values. Among the shapes, SQ had the lowest *SEA*, while CR and MC12 displayed higher *SEA* levels, respectively. For MC12+ and MC20, the *SEA* trend proved more complex, featuring two local maximum values nearly equal in peak, as depicted in Figures 11(d) and 11(e).

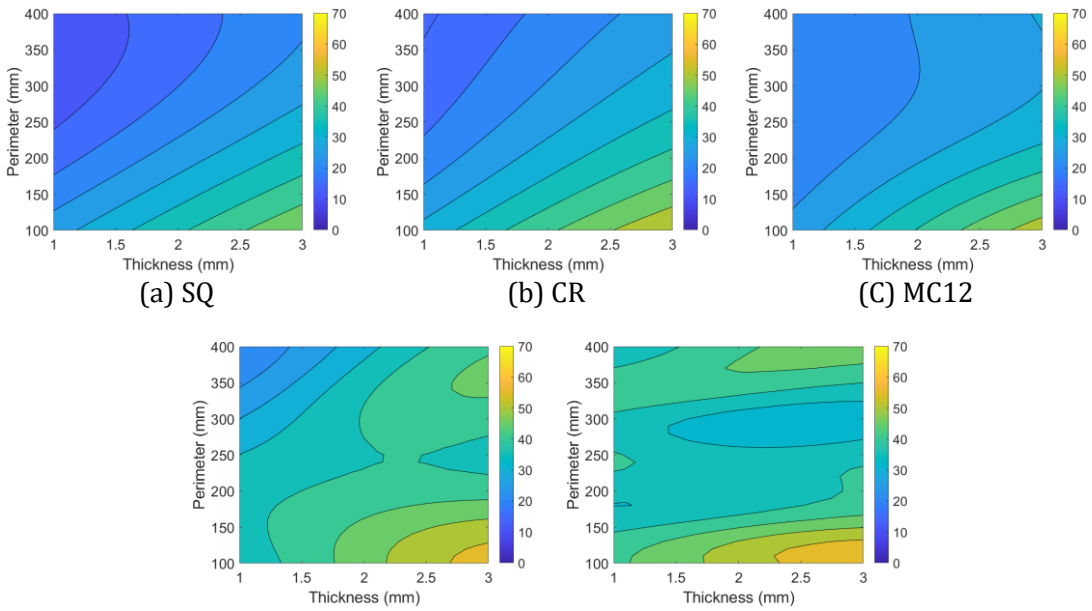

(a) SQ (b) CR (C) MC12

(d) MC12+ (e) MC20

Figure 11 GPR plots for the ***SEA*** of the five cross-sectional shapes

Comparison all five shapes, SQ had the lowest *SEA* while MC20 achieved the highest *SEA*. This outcome showed that given the same energy absorption, each configuration's deformed mass varied, resulting in differing *SEA* values. The *SEA* criterion is critical in crash box structures to minimize collision-induced damage. In such structures, corners act as

primary energy absorption points, making designs with more corners preferable, as these increased *SEA* values by reducing deformed mass. Therefore, the crash box's cross-sectional shape substantially affected energy absorption effectiveness. Even with an identical number of corners, the precise shape needed careful design, as shown by the differing performances of MC12 and MC12+.

4.1.4. Comparison Based on P_m, *CFE*, *SEA*

Table 3 summarized the optimal designs across various crashworthiness performance metrics (P_m, *CFE*, and *SEA*) for each cross-section. Analysis of the surface and contour plots for P_m, *CFE*, and *SEA*, as depicted in Figures 7, 10, and 11, respectively, indicated a clear conflict among the three parameters. The MC20 configuration achieved the highest values for P_m, *CFE*, and *SEA*. Although simpler cross-sections such as SQ and CR were easier to manufacture, the sections proved less efficient at impact energy absorption than MC12+ and MC20. A clear trade-off existed between manufacturability and crashworthiness in crash box design. However, selecting the exact geometry for multi-corner crash box designs required careful consideration.

Table 3 Optimized values of $\boldsymbol{P_m}$, ***CFE***, and ***SEA***, and the corresponding configuration for all cross-sections

Crash box	Parameter	Value	Configuration
Square	P_m (kN)	212	ζ: 400 mm, Δ: 3 mm
	CFE	0.74	ζ: 120 mm, Δ: 3 mm
	SEA (kJ/kg)	48.37	ζ: 120 mm, Δ: 3 mm
Circular	P_m (kN)	241	ζ: 400 mm, Δ: 3 mm
	CFE	0.74	ζ: 120 mm, Δ: 3 mm
	SEA (kJ/kg)	52.49	ζ: 120 mm, Δ: 3 mm
MC12	P_m (kN)	252	ζ: 400 mm, Δ: 3 mm
	CFE	0.73	ζ: 120 mm, Δ: 3 mm
	SEA (kJ/kg)	50.49	ζ: 120 mm, Δ: 3 mm
MC12+	P_m (kN)	388	ζ: 400 mm, Δ: 3 mm
	CFE	0.70	ζ: 120 mm, Δ: 3 mm
	SEA (kJ/kg)	57.80	ζ: 120 mm, Δ: 3 mm
MC20	P_m (kN)	425	ζ: 400 mm, Δ: 3 mm
	CFE	0.74	ζ: 120 mm, Δ: 3 mm
	SEA (kJ/kg)	60.97	ζ: 120 mm, Δ: 3 mm

4.2. Bayesian optimization of the maximum P_m 20-corners crash box

Based on the results from Section 4.1, the GPR-based design exploration identified MC20 as the most efficient geometry in terms of P_m, *CFE*, and *SEA*, surpassing other shapes in several design aspects. The design exploration maintained a fixed cross-sectional shape, optimizing only thickness and perimeter. Consequently, further performance improvements for the MC20 crash box remained feasible through additional optimization. Bayesian optimization was subsequently performed to enhance MC20's performance by keeping the optimized thickness and perimeter values (ζ = 400 mm and Δ = 3 mm) fixed and adjusting the length of each wall segment, as shown in Figure 12(a).

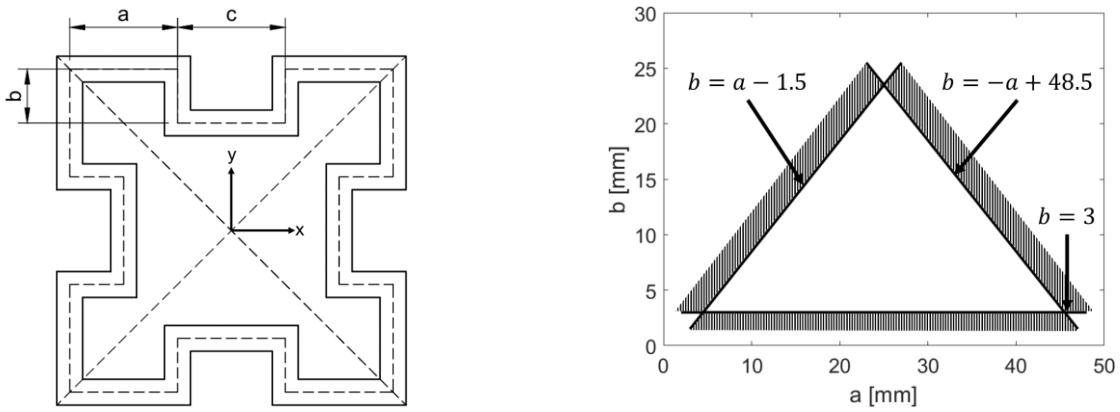

(a) Design Variables (b) Design space for the fine-tuning

Figure 12 Design variables and design space for the fine-tuning of the MC20 geometry using Bayesian optimization with maximum $\boldsymbol{P_m}$ as objectives

Figure 12(a) showed the design variables used to fine-tune the MC20 shape, represented by dimensions *a*, *b*, and *c*. These lengths referred to the mid-plane of the walls, with the crash box symmetrical along the x- and y-axes. The total length of all sides was required to equal 400 mm, establishing a relationship among the three variables. Dimensions a and b were selected as design variables, while c remained dependent which yielded the equation:

$$a + b \leq 50 - 0.5c \tag{12}$$

The minimum value of c was set to Δ to prevent segment overlap, giving the condition $c \geq \Delta$. Therefore, Equation 12 was formulated as follows.

$$b \leq -a + 48.5 \tag{13}$$

To avoid interference between wall segments, *b* plus half the wall thickness was set to be less than a such that there was no interference between wall segments, or:

$$b + \Delta/2 \leq a \quad \text{or} \quad b \leq a - 1.5 \tag{14}$$

From Equations 12, 13, and 14, the design space for maximizing P_m was defined as the area within the triangular region shown in Figure 12(b).

As discussed in Sections 4.1, the thickness and the perimeter of optimized MC20 were ζ = 400 mm and Δ = 3 mm. For this configuration, the corresponding variables for the baseline design were a = 25 mm and b = 12.5 mm, represented by blue square shape in Figure 13. The optimization began with ten random samples, indicated by black circles. Most initial samples appeared in blue contours, suggesting room for further improvement. Adding ten more samples in the orange to red areas marked an enhancement in the crash box dimensions, increasing the P_m value. This process identified the optimal sample with the highest P_m value, represented by the green diamond shape. Figure 13 showed the baseline design, all generated designs, and the best P_m design within the design space. Significantly, the baseline P_m for the MC20, shown as the blue square, was positioned close to the optimized P_m design (MC20-OP_m). Performance comparisons in Figure 14 showed that the optimized design achieved a 7.6% increase in P_m over the baseline. Table 4 outlined additional performance gains with *CFE* and *SEA* increasing by 7.85% and 7.9%, respectively.

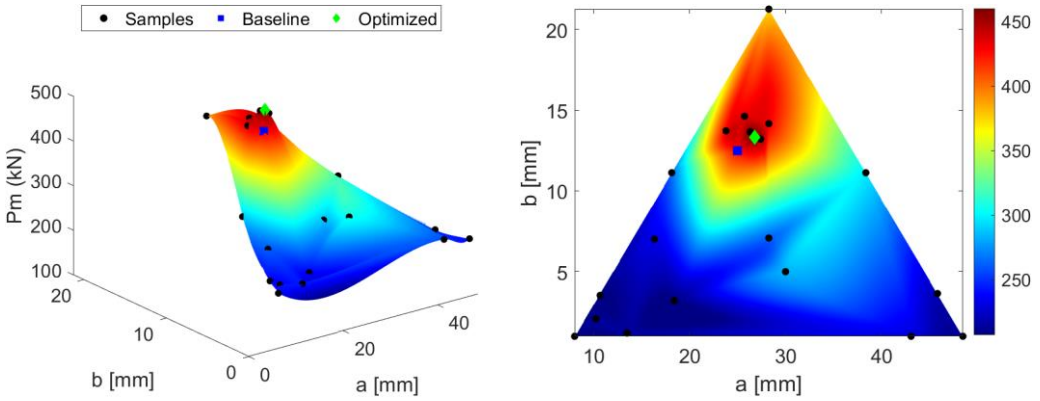

Figure 13 The surface and contour plot for the optimization of the MC20 design to maximize $\boldsymbol{P_m}$. Baseline (blue square shape), Samples (black circle shape), Optimum (green diamond shape)

The geometries of the baseline and optimized designs as shown in Figure 14 suggested longer sides *a* and *b* in the optimized version, contributing to improvements across all criteria. As depicted in Figure 15, the optimized design exhibited better energy absorption than the baseline, benefiting from a progressive buckling mode essential for crashworthiness. These results underscored Bayesian optimization's ability to refine the MC20 design further, with side length adjustments significantly enhancing the 20-corner configuration's performance.

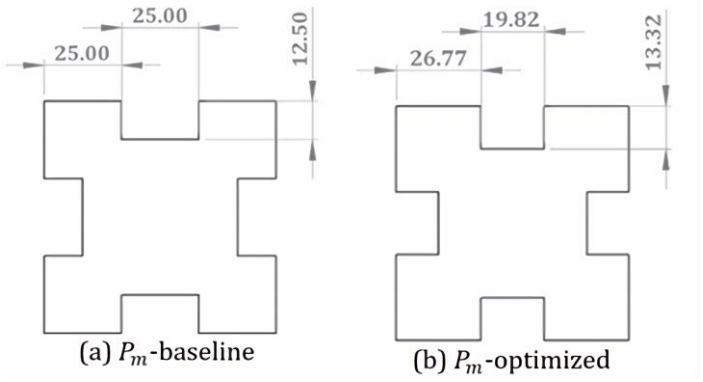

Figure 14 The $\boldsymbol{P_m}$ 20-corner design (baseline and optimized). The dimensions are in millimeters

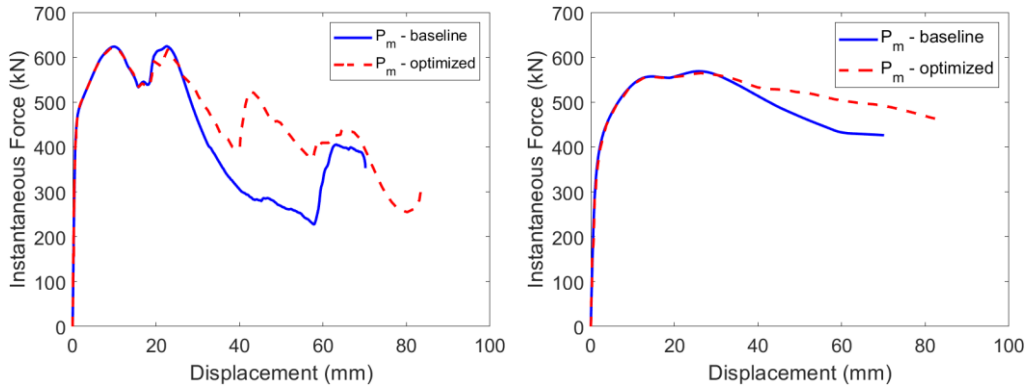

(a) Instantaneous force. (b) Cumulative mean crushing force.

Figure 15 Instantaneous and cumulative mean crushing force for the $\boldsymbol{P_m}$-baseline and the $\boldsymbol{P_m}$-optimized 20 corners crash box geometry

Table 4 Performance comparison between the P_m-baseline and the P_m-optimized 20-corner design. The two designs experienced progressive buckling

Model	a (mm)	b (mm)	c (mm)	P_m (kN)	CFE	SEA (kJ/kg)
Baseline	25.00	12.50	25.00	425	0.68	46.99
Optimized	26.77	13.32	19.82	460	0.74	51.04

4. Conclusions and Future Works

In conclusion, the design exploration and optimization of crash box with various cross-sections which focused on multi-corner designs were successfully conducted. This exploration varied the thickness and perimeter across five cross-sectional shapes namely square (SQ), circular (CR), 12-corner H-like shape (MC12), 12-corner plus-sign shape (MC12+), and 20-corner (MC20). The GPR surrogate model was applied to construct response surfaces for P_m, CFE, and SEA. The results outlined a significant trade-off among the three performance measures, offering valuable insights for designers to consider when developing crash box for real-world applications. The following main conclusions can be drawn (i) the cross-sectional geometry significantly influenced crashworthiness performance with the MC20 configuration achieving the best P_m, CFE, and SEA values compared to other configurations. Therefore, the study concluded that the MC20 configuration was the most efficient among the other configurations; (ii) GPR proved advantageous in the optimization process, offering flexibility for complex nonlinear functions, reducing computational costs, and providing error predictions to further refine the optimization model; and (iii) optimization of the MC20 configuration using the GPR surrogate model focused on a single objective which was to maximizing P_m. This was achieved by fine-tuning the cross-sectional side dimensions while maintaining constant thickness and perimeter. The fine-tuning stage proved crucial in enhancing the P_m, making the stage the most crucial stage in the optimization process. As detailed in this study, the optimized MC20 configuration approximately an 8% improvement in both SEA and CFE. In real vehicles, the main structures positioned behind the crash box and these structures were not entirely rigid. Higher energy absorption and resistance to crushing force could reduce deformation in the main structure, lowering risks for vehicle occupants. For future works, a promising direction would be to optimize the cross-section topology instead of selecting from a limited set of shapes. A free-form approach could identify the optimal cross-section design. Another research avenue could includes studying and optimizing multi-corner crash box performance under uncertainties, such as manufacturing errors or variations in loading direction.

Acknowledgements

Annisa Jusuf and Pramudita Satria Palar were funded in part through the Penelitian, Pengabdian kepada Masyarakat dan Inovasi ITB scheme (P2MI 2024) administered by Institut Teknologi Bandung, Indonesia.

References

Abbasi, M., Reddy, S., Ghafari-Nazari, A., Fard, M., 2015. Multiobjective Crashworthiness Optimization of Multi-Cornered Thin-Walled Sheet Metal Members. *Thin-walled Structures*, Volume 89, pp. 31–41. https://doi.org/10.1016/j.tws.2014.12.009

Abedrabbo, N., Mayer, R., Thompson, A., Salisbury, C., Worswick, M., Riemsdjik, I., 2009. Crash Response of Advanced High-Strength Steel Tubes: Experiment and Model.

International Journal of Impact Engineering, Volume 36(8), pp. 1044–1057. https://doi.org/10.1016/j.ijimpeng.2009.02.006

Abramowicz, W., Jones, N., 1986. Dynamic Progressive Buckling of Circular and Square Tubes. *International Journal of Impact Engineering*, Volume 4(4), pp. 243–270. https://doi.org/10.1016/0734-743X(86)90017-5

Abramowicz, W., Wierzbicki, T., 1989. Axial Crushing of Multicorner Sheet Metal Columns. *Applied Mechanics*, Volume 56(1), pp. 113–120. https://doi.org/10.1115/1.3176030

Alkbir, M., Sapuan, S., Nuraini, A., Ishak, M., 2014. Effect of Geometry on Crashworthiness Parameters of Natural Kenaf Fibre Reinforced Composite Hexagonal Tubes. *Material and Design*, Volume 60, pp. 85–93. https://doi.org/10.1016/j.matdes.2014.02.031

Bastien, C., 2014. The Prediction of Kinematics and Injury Criteria of Unbelted Occupants Under Autonomous Emergency Braking, Coventry University

Bhutda, S., Sonje, S., Goel, M.D., 2023. Multi-Objective Optimization of Foam-Filled Tubes to Enhance the Crashworthiness Characteristics Under Impact Loading. *Journal of the Brazilian Society of Mechanical Sciences and Engineering*, Volume 45(9), p. 483. https://doi.org/10.1007/s40430-023-04398-1.

Borse, A., Gulakala, R., Stoffel, M., 2024. Multi-Parameter Design Optimization of Crash Box for Crashworthiness Analysis. *Proceedings in Applied Mathematics and Mechanics*, p. e202400096. https://doi.org/10.1002/pamm.202400096.

Chen, T., Zhang, Y., Lin, J., Lu, Y., 2019. Theoretical Analysis and Crashworthiness Optimization of Hybrid Multi-Cell Structures. *Thin-walled Structures*, Volume 142, pp. 116–131. https://doi.org/10.1016/j.tws.2019.05.002

Cheng, J.C., 2011. Twelve-Cornered Strengthening Member. United States, Patent No. 9533710.

Christensen, J., 2022. Efficient Crash Structure Design for Road Traffic Accidents of Tomorrow. *International Journal of Crashworthiness*, Volume 28(5), pp. 629–648. https://doi.org/10.1080/13588265.2022.2114577

Ciampaglia, A., Fiumarella, D., Niutta, C.B., Ciardiello, R., Belingardi, G., 2021. Impact Response of an Origami-Shaped Composite Crash Box: Experimental Analysis and Numerical Optimization. *Composite Structures*, Volume 256, p. 113093. https://doi.org/10.1016/j.compstruct.2020.113093

Dimas, A., Dirgantara, T., Gunawan, L., Jusuf, A., and Putra, I.S., 2014. The Effects of Spot Weld Pitch to the Axial Crushing Characteristics of Top-Hat Crash Box. *Applied Mechanics and Materials*, Volume 660, pp. 578–582. http://dx.doi.org/10.4028/www.scientific.net/AMM.660.578

Djamaluddin, F., 2024. Optimization of Foam-Filled Crash-Box Under Axial Loading For Pure Electric Vehicle. *Results in Materials*, Volume 21, p. 100505. https://doi.org/10.1016/j.rinma.2023.100505

Fang, J., Sun, G., Qiu, N., Kim, N. H., Li, Q., 2017. On Design Optimization for Structural Crashworthiness and its State of the Art. *Structural and Multidisciplinary Optimization*, Volume 55, pp. 1091–1119. https://doi.org/10.1007/s00158-016-1579-y

Galib, D.A., Limam, A., 2004. Experimental and Numerical Investigation of Static and Dynamic Axial Crushing of Circular Aluminum Tubes. *Thin-walled Structures*, Volume 42(8), pp. 1103–1137. https://doi.org/10.1016/j.tws.2004.03.001

Godat, A., Legeron, F., Bazonga, D., 2012. Stability Investigation of Local Buckling Behavior of Tubular Polygon Columns Under Concentric Compression. *Thin-walled Structures*, Volume 53, pp. 131–140. https://doi.org/10.1016/j.tws.2011.12.013

Gunawan, L., 2013. Material Characterization and Axial Crushing Tests of Single and Double-Walled Columns at Intermediate Strain Rates. *Journal of Mechanical Engineering,* Volume 10(2), pp. 19–36

Halton, J.H., 1964. Algorithm 247: Radical-Inverse Quasi-Random Point Sequence. *Communications of the ACM*, Volume 7(12), pp. 701–702. https://doi.org/10.1145/355588.365104

Hou, S., Li, Q., Long, S., Yang, X., Li, W., 2007. Design Optimization of Regular Hexagonal Thin-Walled Columns with Crashworthiness Criteria. *Finite Elements in Analysis and Design*, Volume 43(6-7), pp. 555–565. https://doi.org/10.1016/j.finel.2006.12.008

Hou, W., He, P., Yang, Y., Sang, L., 2023. Crashworthiness Optimization of Crash Box with 3D-printed Lattice Structures. *International Journal of Mechanical Sciences*, Volume 247, p. 101819. https://doi.org/10.1016/j.ijmecsci.2023.108198

Hull, D., 1991. A Unified Approach to Progressive Crushing of Fibre-Reinforced Composite Tubes. *Composites Science and Technology*, Volume 40(4), pp. 377–421. https://doi.org/10.1016/0266-3538(91)90031-J

Jones, D., Schonlau, M., Welch, W., 1998. Efficient Global Optimization of Expensive Black-Box Functions. *Journal of Global Optimization,* pp. 455–492. https://doi.org/10.1023/A:1008306431147

Jongpradist, P., Tongthong, S., Kongwat, S., Ruangjirakit, K., Thongchom, C., Hasegawa, H., 2024. Optimizing Functionally Graded Hexagonal Crash Boxes with Honeycomb Filler For Enhanced Crashworthiness. *Structures*, Volume 59, p. 105775. https://doi.org/10.1016/j.istruc.2023.105775

Jusuf, A., Allam, F.S., Dirgantara, T., Gunawan, L., Putra, I.S., 2011. Low Velocity Impact Analyses of Prismatic Columns Using Finite Element Method. *Key Engineering Materials*, Volume 462-463, pp. 1308–1313. http://dx.doi.org/10.4028/www.scientific.net/KEM.462-463.1308

Jusuf, A., Dirgantara, T., Gunawan, L., Putra, I., 2015. Crashworthiness Analysis of Multi-Cell Prismatic Structures. *International Journal of Impact Engineering*, Volume 78, pp. 34–50. https://doi.org/10.1016/j.ijimpeng.2014.11.011

Kholil, A., Kiswanto, G., Farisi, A. A., Istiyanto, J., 2023. Finite Element Analysis of Lattice Structure Model with Control Volume Manufactured Using Additive Manufacturing. *International Journal of Technology*, Volume 14(7), pp. 1428–1437. https://doi.org/10.14716/ijtech.v14i7.6660

Kumar, A.P., Maneiah, D., 2019. Deformation Studies on the Significance of Combined Geometry Tubes as Energy Absorbing Structures. *International Journal of Civil Engineering and Technology*, Volume 10(1), pp. 2812–2820.

Kumar, A.P., Sankar, L.P., Maneiah, D., Upendra, G., 2019. Lateral Crushing and Energy Absorption Behavior of Multicellular Tube Structures. *International Journal of Innovative Technology and Exploring Engineering*, Volume 9(1), pp. 2684—2687. http://dx.doi.org/10.35940/ijitee.A4837.119119

Liu, S., Tong, Z., Tang, Z., Liu, Y., Zhang, Z., 2015. Bionic Design Modification of Non-Convex Multi-Corner Thin-Walled Columns for Improving Energy Absorption Through Adding Bulkheads. *Thin-walled Structures*, Volume 88, pp. 70–81. https://doi.org/10.1016/j.tws.2014.11.006

Liu, Y., 2008. Crashworthiness Design of Multi-Corner Thin-Walled Columns. *Thin-Walled Structures,* Volume 46(12), pp. 1329–1337. https://doi.org/10.1016/j.tws.2008.04.003

Liu, Y., Day, M., 2007. Development of Simplified Finite Element Models for Straight Thin-Walled Tubes with Octagonal Cross Section. *International Journal of Crashworthiness*, Volume 12(5), pp. 503–508. https://doi.org/10.1080/13588260701483557

Liu, Z., Huang, Z., Qin, Q., 2017. Experimental and Theoretical Investigations on Lateral Crushing of Aluminum Foam-Filled Circular Tubes. *Composite Structures*, Volume 175, pp. 19–27. https://doi.org/10.1016/j.compstruct.2017.05.004

Lu, Q., Deng, X., Liu, F., 2023. Crashworthiness Study of A Novel Radial Gradient Multicell Tube. *Journal of the Brazilian Society of Mechanical Sciences and Engineering*, Volume 45(8), p. 409. https://doi.org/10.1007/s40430-023-04319-2

Lu, R., Liu, X., Chen, S., Hu, X., Liu, L. 2017. Axial Crushing Analysis for Tailor Rolled Square Tubes With Axially Graded Both Wall Thickness And Material. *Thin-walled structures,* Volume 117, pp. 10–24. https://doi.org/10.1016/j.tws.2017.04.001

Mamalis, A., Manolakos, D., Ioannidis, M., Papapostolou, D., 2004. Crashworthiness Characteristics of Axially Statically Compressed Thin-Walled Square CFRP Composite Tubes: Experimental. *Composite Structures*, Volume 63(3-4), pp. 347–360. https://doi.org/10.1016/S0263-8223(03)00183-1

Nagarjun, J., Kumar, A.P., Reddy, K.Y., Sankar, L.P., 2020. Dynamic Crushing and Energy Absorption Perfromance of Newly Designed Multitubular Structures. *Materials Today: Proceedings*, Volume 27, pp. 1928–1933. https://doi.org/10.1016/j.matpr.2020.04.103

Nakazawa, Y., Tamura, K., Yoshida, M., Takagi, K., Kano, M., 2005. Development of Crash-Box for Passenger Car with High Capability for Energy Absorption. Barcelona, VIII International Conference on Computational Plasticity.

Olabi, A., Morris, E., Hashmi, M., 2007. Metallic Tube Type Energy Absorbers: A Synopsis. *Thin-walled Structures*, Volume 45(7-8), pp. 706–726. https://doi.org/10.1016/j.tws.2007.05.003

Palar, P.S., Shimoyama, K., 2019. Kriging with Composite Kernel Learning for Surrogate Modeling in Computer Experiments. San Diego, California, AIAA SciTech Forum. http://dx.doi.org/10.2514/6.2019-2209

Palar, P.S., Zuhal, L.R., Shimoyama, K., 2020. Gaussian Process Surrogate Model with Composite Kernel Learning for Engineering Design. *AIAA Journal*, Volume 58(4), pp. 1864–1880. https://doi.org/10.2514/1.J058807

Pirmohammad, S., Esmaeili-Marzdashti, S., 2019. Multi-Objective Crashworthiness Optimization of Square and Octagonal Bitubal Structures Including Different Hole Shapes. *Thin-walled structures*, Volume 139, pp. 126–138. https://doi.org/10.1016/j.tws.2019.03.004

Qi, C., Yang, S., Dong, F., 2012. Crushing Analysis and Multiobjective Crashworthiness Optimization Of Tapered Square Tubes Under Oblique Impact Loading. *Thin-Walled Structures*, Volume 59, pp. 103–119. https://doi.org/10.1016/j.tws.2012.05.008

Rasmussen, C., 2003. Gaussian Processes In Machine Learning. In: Summer School on Machine Learning. *Springer*, Volume 3176, pp. 63–71. https://doi.org/10.1007/978-3-540-28650-9_4

Reddy, S., Abbasi, M., Fard, M., 2015. Multi-Cornered Thin-Walled Sheet Metal Members for Enhanced Crashworthiness and Occupant Protection. *Thin-walled structures*, Volume 94, pp. 56–66. https://doi.org/10.1016/j.tws.2015.03.029

Reuter, C., Tröster, T., 2017. Crashworthiness and Numerical Simulation of Hybrid Aluminium-CFRP Tubes Under Axial Impact. *Thin-Walled Structures*, Volume 117, pp. 1–9. https://doi.org/10.1016/j.tws.2017.03.034

Schneider, F., Jones, N., 2003. Influence of Spot-Weld Failure on Crushing of Thin-Walled Structural Sections. *International Journal of Mechanical Sciences*, Volume 45(12), pp. 2061–2081. https://doi.org/10.1016/j.ijmecsci.2003.11.004

Seek, C.Y., Kok, C.K., Lim, C.H., Liew, K.W., 2022. A Novel Lattice Structure for Enhanced Crush Energy Absorption. *International Journal of Technology*, Volume 13(5), pp. 1139–1148. http://dx.doi.org/10.14716/ijtech.v13i5.5829

Shahi, V., Marzbanrad, J., 2012. Analytical and Experimental Studies On Quasi-Static Axial Crush Behavior of Thin-Walled Tailor-Made Aluminum Tubes. *Thin-walled structures*, Volume 60, pp. 24–37. https://doi.org/10.1016/j.tws.2012.05.015

Skhvediani, A., Rodionova, M., Savchenko, N., Kudryavtseva, T., 2023. Prediction of the Road Accidents Severity Level: Case of Saint-Petersburg and Leningrad Oblast. *International Journal of Technology*, Volume 14(8), pp. 1717–1727. https://doi.org/10.14716/ijtech.v14i8.6859

Tang, Z., Liu, S., Zhang, Z., 2012. Energy Absorption Properties of Non-Convex Multi-Corner Thin-Walled Columns. *Thin-walled structures*, Volume 51, pp. 112–120. https://doi.org/10.1016/j.tws.2011.10.005

Tarigopula, V., Langseth, M., Hopperstad, O., Clausen, A., 2006. Axial Crushing of Thin-Walled High-Strength Steel Sections. *International Journal of Impact Engineering*, Volume 32(5), pp. 847–882. https://doi.org/10.1016/j.ijimpeng.2005.07.010.

Wang, W., Dai, S., Zhao, W., Wang, C., 2022. Multi-Objective Optimization of Hexahedral Pyramid Crash Box Using Moea/D-Dae Algorithm. *Applied soft computing*, Volume 118, p. 108481. https://doi.org/10.1016/j.asoc.2022.108481

Wang, Z., Jin, X., Li, Q., Sun, G., 2020. On Crashworthiness Design of Hybrid Metal-Composite Structures. *International Journal of Mechanical Sciences*, Volume 171, p. 105380. https://doi.org/10.1016/j.ijmecsci.2019.105380

White, M., Jones, N., 1999. Experimental Quasi-Static Axial Crushing of Top-Hat and Double-Hat Thin-Walled Sections. *International Journal of Mechanical Sciences*, Volume 41(2), pp. 179–208. https://doi.org/10.1016/S0020-7403(98)00047-2

Wu, S., Sun, G., Wu, X., Li, G., Li, Q., 2017. Crashworthiness Analysis and Optimization of Fourier Varying Section Tubes. *International Journal of Non-linear Mechanics*, Volume 92, pp. 41–58. https://doi.org/10.1016/j.ijnonlinmec.2017.03.001

Xu, F., Sun, G., Li, G., Li, Q., 2014. Experimental Study on Crashworthiness Of Tailor-Welded Blank (TWB) Thin-Walled High-Strength Steel (HSS) Tubular Structure. *Thin-walled structures*, Volume 74, pp. 12–27. https://doi.org/10.1016/j.tws.2013.08.021

Yamashita, M., Gotoh, M., Sawairi, Y., 2003. Axial Crush of Hollow Cylindrical Structures with Various Polygonal Cross-Sections: Numerical Simulation and Experiment. *Journal of Materials Processing Technology*, Volume 140(1-3), pp. 59–64. https://doi.org/10.1016/S0924-0136(03)00821-5

Yuan, L., Shi, H., Ma, J., You, Z., 2019. Quasi-Static Impact of Origami Crash Boxes with Various Profiles. *Thin-Walled Structures,* Volume 141, pp. 435–446. https://doi.org/10.1016/j.tws.2019.04.028

Zhang, J., Zheng, D., Lu, B., Liu, Q., 2022. A Numerical and Theoretical Study on Crushing Behaviours of Variable Thickness 12 Right-Angles Section Tubes. *International journal of Crashworthiness*, Volume 27(1), pp. 168–180. https://doi.org/10.1080/13588265.2020.1784538

Zhang, X., Huh, H., 2010. Crushing Analysis of Polygonal Columns and Angle Elements. *International Journal of Impact Engineering*, Volume 37(4), pp. 441–451. https://doi.org/10.1016/j.ijimpeng.2009.06.009

Zhang, X., Wen, Z., Zhang, H., 2014. Axial Crushing and Optimal Design of Square Tubes With Graded Thickness. *Thin-walled Structures*, Volume 84, pp. 263–274. https://doi.org/10.1016/j.tws.2014.07.004

Zhang, X., Zhang, H., 2012. Experimental and Numerical Investigation on Crush Resistance of Polygonal Columns and Angle Elements. *Thin-walled Structures*, Volume 57, pp. 25–36. https://doi.org/10.1016/j.tws.2012.04.006

Zhang, X., Zhang, H., Yang, C., Leng, K., 2019. Static and Dynamic Axial Crushing of Self-Locking Multi-Cell Tubes. *International Journal of Impact Engineering*, Volume 127, pp. 17–30. https://doi.org/10.1016/j.ijimpeng.2019.01.002

Zhou, C., Zhou, Y., Wang, B., 2017. Crashworthiness Design for Trapezoid Origami Crash Boxes. *Thin-walled Structures*, Volume 117, pp. 257–267. https://doi.org/10.1016/j.tws.2017.03.022